Assessment of Laminar, Convective Aeroheating Prediction Uncertainties for Mars-Entry Vehicles

Brian R. Hollis*

NASA Langley Research Center, Hampton, Virginia 23681

and

Dinesh K. Prabhu[†]

ERC Corporation, Mountain View, California 94035

An assessment of computational uncertainties is presented for numerical methods used by NASA to predict laminar, convective aeroheating environments for Mars-entry vehicles. A survey was conducted of existing experimental heat transfer and shock-shape data for high-enthalpy reacting-gas CO_2 flows, and five relevant test series were selected for comparison with predictions. Solutions were generated at the experimental test conditions using NASA state-of-the-art computational tools and compared with these data. The comparisons were evaluated to establish predictive uncertainties as a function of total enthalpy and to provide guidance for future experimental testing requirements to help lower these uncertainties.

Nomenclature

H_w	=	wall enthalpy, J/kg
H_0	=	total freestream enthalpy, J/kg
L/D	=	lift-to-drag ratio
K_c	=	equilibrium constant, — or $gmol/cm^3$
k_b	=	backward reaction rate coefficient, $cm^3/gmol \cdot s$ or $cm^6/gmol^2 \cdot s$
k_f	=	forward reaction rate coefficient, $cm^3/gmol \cdot s$
M_∞	=	freestream Mach number
q_w	=	heat transfer rate at the wall, W/m^2
R_C	=	corner radius, m
$Re_{\infty,D}$	=	freestream Reynolds number based on diameter, $\rho_\infty U_\infty D/\mu_\infty$
R_{max}	=	maximum radius, m
R_N	=	hemispherical nose radius, m
T_∞	=	freestream temperature, K
U_∞	=	freestream velocity, m/s
z	=	Cartesian distance from nose along symmetry plane, m
α	=	angle of attack, deg
θ	=	cone angle, deg
ρ_∞	=	freestream density, kg/m^3

I. Introduction

TWO important goals for NASA's future Mars exploration programs are to perform a robotic sample return mission and to enable human exploration missions. Both goals require the safe landing of much greater masses (in excess of 10 t) than those of previous Mars missions. However, the heritage technology employed in past NASA missions from Viking to Mars Science Laboratory (MSL), that of a rigid, 70 deg sphere-cone, ablative thermal protection system (TPS), will not be sufficient to accomplish such new missions. Thus, an Entry, Descent, and Landing Systems Analysis Study (EDL-SA) was conducted [1] that defined three entry-vehicle architectures that could provide the required increased mass capability. These high-mass, mars-entry system (HMMES) architectures are 1) a midrange lift-to-drag ratio ($L/D = 0.4$–0.6) vehicle with a rigid aeroshell; 2) a large, hypersonic and/or supersonic inflatable aerodynamic decelerator system (HIADS and SIADS) for high-altitude aerobraking; and 3) hypersonic and/or supersonic retropropulsion. Mixed architectures that consist of combinations of these elements were also considered. In Fig. 1, these three main vehicle classes are shown as architectures 1–3, and various combinations thereof are shown as architectures 4–8. Conceptual illustrations for the mid-L/D aeroshell, inflatable aerodynamic decelerator, and hypersonic/supersonic retropropulsion system are shown in Figs. 2–4.

To insure the safety and success of such missions, the uncertainties in the modeling and prediction of the aerothermodynamic environment, which includes the surface heat transfer, pressure and shear, and the integrated aerodynamic forces and moments that the entry vehicle will experience, must be defined. A step toward fulfilling this requirement is presented in this study, which was performed as part of a larger activity [2] sponsored by NASA's Fundamental Aeronautics Program, Hypersonics Project to define, and ultimately reduce, aerothermodynamic uncertainties for several hypersonic mission types. A variety of physical phenomena that influence the HMMES aerothermodynamic environment have been identified. These include, but are not limited to the following: boundary-layer transition; TPS blowing, ablation, and roughness; shock-layer radiation; flexible structure/flowfield interactions; retropropulsion thruster and reaction control system jet/flowfield and jet/surface interactions; noncontinuum effects at high altitude and in separated wake flows; surface catalysis; nonequilibrium gas kinetics, etc. A discussion of many of these phenomena and of computational methods used for modeling them is presented in [3]. The *sensitivities* of these computational methods to input parameters for numerical models of physical phenomena (as distinct from *uncertainties* determined through comparison with experimental data, which is the subject of this report) have been explored in [4].

The current study is limited to uncertainties in the prediction of laminar, attached high-enthalpy flow of CO_2 over smooth, nonablating surfaces. These restrictions define the most basic validation case (short of perfect-gas flow) relevant to Mars missions. Without a thorough understanding of the computational uncertainties in the modeling of these phenomena, uncertainties in modeling other phenomena, such as turbulence, roughness, and radiation, cannot properly be addressed.

Fig. 1 HMMES architecture options.

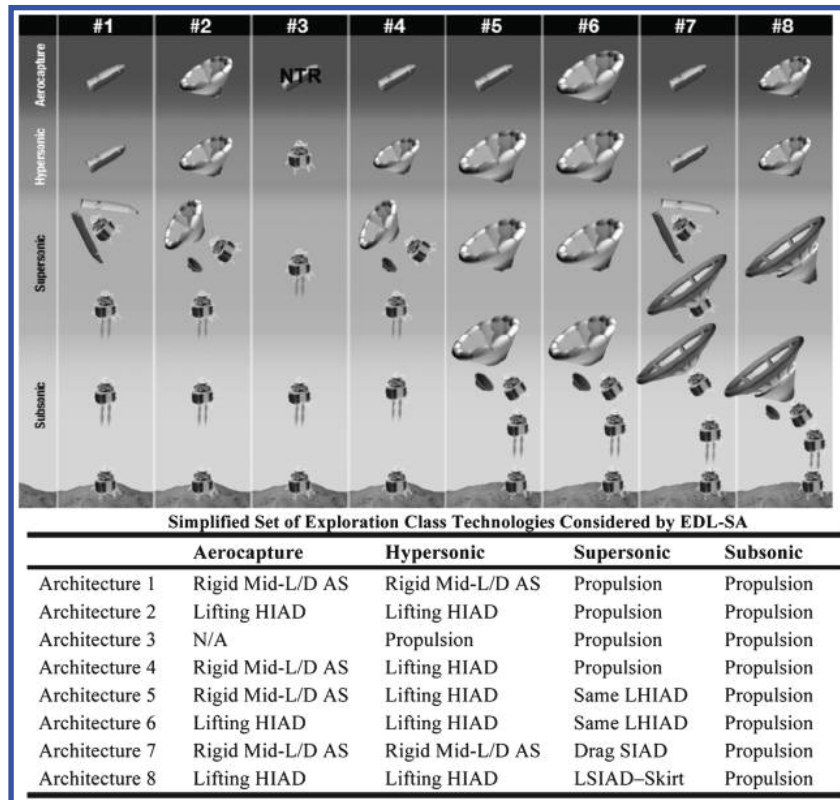|	Aerocapture	Hypersonic	Supersonic	Subsonic
Architecture 1	Rigid Mid-L/D AS	Rigid Mid-L/D AS	Propulsion	Propulsion
Architecture 2	Lifting HIAD	Lifting HIAD	Propulsion	Propulsion
Architecture 3	N/A	Propulsion	Propulsion	Propulsion
Architecture 4	Rigid Mid-L/D AS	Lifting HIAD	Propulsion	Propulsion
Architecture 5	Rigid Mid-L/D AS	Lifting HIAD	Same LHIAD	Propulsion
Architecture 6	Lifting HIAD	Lifting HIAD	Same LHIAD	Propulsion
Architecture 7	Rigid Mid-L/D AS	Rigid Mid-L/D AS	Drag SIAD	Propulsion
Architecture 8	Lifting HIAD	Lifting HIAD	LSIAD–Skirt	Propulsion

Fig. 2 Mid-L/D rigid aeroshell.

The approach followed to define the uncertainties for laminar, attached high-enthalpy CO_2 flows was as follows:

1) Identify relevant sources of experimental data (i.e., high-enthalpy surface and flowfield test data obtained in CO_2 flows). For simplicity, only 0 deg angle-of-attack data were considered.

2) Generate flowfield predictions at the selected test conditions using the state-of-the-art computational tools currently employed in the development of NASA's Mars missions. Although computations may have been previously performed for some data sets using older software packages, it is important to emphasize that, for the purposes of the current study, new solutions were generated for all cases. The new solutions were generated to ensure that a consistent methodology was applied using the latest software versions. Similarly, although other similar software tools exist outside of NASA and have been employed to model such flows, they were not considered in this study.

3) Perform and assess comparisons between the experimental data and numerical results to determine the current state of the art in

Fig. 3 Inflatable aerodynamic decelerator.

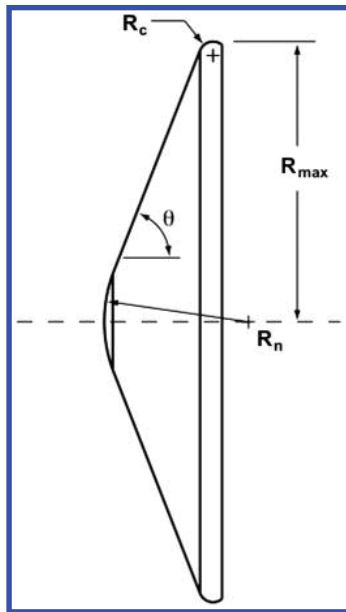Fig. 4 Supersonic retropropulsion system.

Fig. 5 Seventy degree sphere-cone geometry.

computational predictions for laminar high-enthalpy, convective aerothermodynamic environments of Mars missions.

It is expected that the results of this effort to define the state of the art will be used as guidelines for future efforts to reduce the computational uncertainties. Reduction of the modeling uncertainties will require the acquisition of new high-fidelity experimental ground- and flight-test data on both macroscopic aerothermodynamics properties (surface heating and pressure, flowfield structure, aerodynamics forces and moments, boundary-layer transition, etc.) and fundamental physical properties (chemical, vibrational, and electronic excitation and relaxation rates, transport properties, and radiation emission and absorption rates). Concurrent development and validation of advanced computational methods and algorithms will also be required.

II. Review of Experimental Data Applicable to HMMES Missions

A thorough literature search was performed to identify sources of experimental data relevant to the HMMES uncertainty assessment. Data sets were selected for consideration, in which surface heat transfer measurements were performed in pure CO_2 test gas at conditions where postshock chemical reactions were generated (i.e., in excess of 1 MJ/kg). Although the actual composition of the Martian atmosphere is $\sim 95.3\% CO_2$, $2.7\% N_2$, and 2.0% Ar (by volume), the kinetics of CO_2 are expected to be the greatest uncertainty component because of its predominance, and so data sets with N_2 (or other minor components) were left to later consideration. Additional

data that did not meet the current criteria were also noted for future consideration (e.g., turbulent data, high-enthalpy air or N_2 data).

A. Experimental Data Sets for HMMES Laminar, Convective Uncertainty Assessment

Five sources of laminar high-enthalpy, convective heat transfer data in a CO_2 environment were identified for inclusion in this study. These data were obtained in the NASA Ames Research Center (ARC) 42-Inch Shock Tunnel, the General Applied Sciences Laboratories (GASL) HYPULSE Expansion Tube, the Caltech T5 Reflected Shock Tunnel, the University of Illinois Hypervelocity Expansion Tube, and the Calspan University of Buffalo Research Center (CUBRC) LENS I Reflected Shock Tunnel. All data are from 70 deg sphere-cone model geometries (Fig. 5) similar to that of MSL, although there is some variation in nose and corner radius dimensions (relative to the maximum radius) of the models tested.

Test conditions from each of these studies are listed in chronological order in Table 1 and a summary of the wind-tunnel model parameters for each test is provided in Table 2. Note that the conditions listed do not necessarily represent all the data obtained in each facility; for simplicity, the data considered herein were limited to 0 deg angle of attack at laminar conditions. Additional data for nonzero angle of attack and for transitional and turbulent boundary layers are also available in many of these data sets. It is also important to note that these test conditions were actually determined from a combination of experimental flowfield measurements (e.g., shock speed and pitot pressure) and numerical simulation tools (to obtain mass fractions). These numerical tools employ some of the same physical models as do the flowfield codes which are, in theory, to be validated by comparison with the experimental data. Thus, a complete validation exercise, which is outside the scope of this study, would require iterative refinements of test condition predictions and model-in-flow simulations.

The enthalpy/Reynolds number range of the test data is shown in Fig. 6. Total enthalpies ($H_0 - H_{wall}$) ranged from 1.9 (near to perfect gas) to 12.3 MJ/kg (nonequilibrium chemistry). Reynolds numbers (based on diameter) for all data considered were less than 10^6, which resulted in laminar conditions for all cases except one partly transitional run in the CUBRC data set.

For comparison with flight conditions, reference values for HMMES mid-L/D and HIADS configurations are shown on this plot, as well as reference values for the Mars Science Laboratory and Mars Viking missions. It is notable that the MSL reference condition is at the high end of the range of Reynolds number and enthalpy test conditions, whereas the HMMES conditions are a factor of 2 to 3 higher in enthalpy and an order of magnitude greater in Reynolds number. In contrast, the peak heating condition for the Mars Viking mission is well within the range of test conditions.

1. NASA ARC 42-Inch Shock Tunnel Data

Data were obtained [5] at laminar test conditions on a 70 deg sphere-cone model in CO_2, air, and CO_2-Ar environments in the

Table 1   Test conditions

Facility	Facility type	ρ_∞, kg/m³	T_∞, K	U_∞, m/s	$Re_{\infty,D}$	$H_0 - H_w$, MJ/kg	Freestream mass fractions [CO_2]	[CO]	[O_2]	[O]
NASA Ames 42-Inch Shock Tunnel	Reflected shock tunnel	3.10×10^{-4}	200	4150	0.25×10^6	8.5	1.000	0.000	0.000	0.000
GASL HYPULSE (runs 747, 749)	Shock expansion tube	5.79×10^{-3}	1088	4772	0.93×10^6	12.3	1.000	0.000	0.000	0.000
Caltech T5 (run 2256)	Reflected shock tunnel	5.70×10^{-2}	1407	2732	1.67×10^6	6.1	0.831	0.108	0.061	0.000
Caltech T5 (run 2254)	Reflected shock tunnel	3.12×10^{-2}	1828	3367	1.25×10^6	10.6	0.550	0.287	0.151	0.012
Caltech T5 (run 2255)	Reflected shock tunnel	7.83×10^{-2}	2188	3514	2.26×10^6	11.3	0.592	0.259	0.139	0.009
CUBRC LENS I (series 1, run 12)	Reflected shock tunnel	5.26×10^{-4}	691	2761	0.29×10^6	4.9	0.901	0.063	0.036	0.00
CUBRC LENS I (series 2, run 16)	Reflected shock tunnel	1.48×10^{-2}	361	1907	0.94×10^6	1.9	1.000	0.000	0.000	0.000
CUBRC LENS I (series 2, run 12)	Reflected shock tunnel	8.70×10^{-3}	931	2939	0.77×10^6	6.0	0.843	0.100	0.057	0.000
CUBRC LENS I (series 2, run 08)	Reflected shock tunnel	8.96×10^{-3}	892	2870	0.21×10^6	5.6	0.863	0.087	0.05	0.000
CUBRC LENS I (series 2, run 13)	Reflected shock tunnel	6.06×10^{-3}	1116	3373	0.16×10^6	8.6	0.687	0.199	0.110	0.003
University of Illinois HET	Shock expansion tube	1.44×10^{-2}	1172	3058	0.43×10^6	5.7	1.000	0.000	0.000	0.000

Table 2   Wind-tunnel model information

Facility	Max radius, in.	Nose radius, in.	Corner radius, in.	Cone angle, deg	Model instrumentation	Model material	Refs.
NASA Ames 42-Inch Shock Tunnel	$A = 2.74$ $B = 2.82$ $C = 2.99$	$A = 1.5$ $B = 1.5$ $C = 1.5$	$A = 0.039$ $B = 0.167$ $C = 0.470$	70	Surface junction thermocouples	Copper	[5]
GASL HYPULSE	1.00	0.5	MP1 = 0.05 MP3 = 0.10 MP4 = 0.20	70	Thin-film temperature gauges	Macor ceramic	[6–8]
Caltech T5	3.50	1.75	0.35	70	Fast-response coaxial thermocouples	SS304 stainless steel	[9,10]
CUBRC LENS I, series 1	12.0	6.0	0.60	70	Thin-film temperature gauges and coaxial thermocouples	Stainless steel	[11,12]
CUBRC LENS I, series 2	6.0	3.0	0.30	70	Coaxial thermocouples, thin-film temperature gauges, and silver calorimeters	Stainless steel	[13]
University of Illinois HET	1.00	0.5	0.05	70	Fast-response coaxial thermocouples	AI 2024 and A2 tool steel	[14]

NASA ARC 42-Inch Shock Tunnel (also sometimes referred to as the Ames 3.5 ft Shock Tunnel). The facility (since demolished) was a combustion-heated, reflected shock tunnel with 10–20 ms test times. Heat transfer data and flowfield schlieren images were obtained on copper models instrumented with surface thermocouples. Three separate configurations were actually tested. All were 70 deg sphere-cone geometries with 1.5 in. nose radii; however, the model had interchangeable outer sections with various corner radii that resulted in 2.74–2.99 in. maximum radius models. Besides the 0 deg angle-of-attack runs considered herein, additional runs were performed at $\alpha = 10$ and 20 deg. An experimental uncertainty of $\pm 10\%$ was cited for the heating data from this study.

2.   GASL HYPULSE Expansion Tube Data

Testing was performed [6–8] in the GASL (now ATK) HYPULSE Expansion Tube on 70 deg sphere-cone models of 1.00 in. maximum radius in air and CO_2 test gases. Laminar data were obtained on three 70 deg sphere-cone models of varying corner radii and on a blunted hyperboloid with 70 deg asymptotes. The models were fabricated from Macor ceramic and instrumented with thin-film heat-flux gauges. In addition to the $\alpha = 0$ data considered herein, data are also available for 4 and 8 deg angles of attack. An experimental uncertainty of $\pm 11\%$ was cited for the heating data from this study.

3.   Caltech T5 Reflected Shock Tunnel Data

Heat transfer tests were performed [9,10] on a 3.50 in. maximum radius, 70 deg sphere-cone model in the Caltech T5 Reflected Shock

Tunnel in CO_2 and N_2 test gases. The model was fabricated from stainless steel and instrumented with fast-response coaxial thermocouples. Testing was performed at angles of attack of 0, 11, and 16 deg and laminar, transitional, and turbulent data were produced, although only laminar 0 deg runs are considered herein. Although a specific value for experimental uncertainty was not cited for the CO_2 data of [9], error bars shown on the plots were approximately $\pm 11\%$.

4.   CUBRC LENS I Reflected Shock Tunnel Data

Measurements on MSL geometry models were performed in CO_2 in the CUBRC LENS I Reflected Shock Tunnel. Two test series were performed: the first with a thermocouple and thin-film instrumented, 12 in. maximum radius model [11,12] and the second with a 6 in. maximum radius model instrumented with thin-film gauges, coaxial thermocouples, and silver calorimeters [13]. Both models were fabricated from stainless steel. In addition to the 0 deg angle-of-attack data considered herein, runs were also made at $\alpha = 11$, 16, and 20 deg that produced laminar, transitional, and turbulent flows. Although specific values for experimental uncertainties for each gauge type were not given, error bars shown on plots in [13] were approximately ± 5 to $\pm 10\%$.

5.   University of Illinois Hypervelocity Expansion Tube Data

The most recent data available [14] were obtained in the University of Illinois Hypervelocity Expansion Tube (HET). The test geometry was a 1.00 in. maximum radius, 70 deg sphere-cone stainless steel model instrumented with fast-response coaxial thermocouples. Laminar data were obtained at angles of attack of 0, 11, and 16 deg. An uncertainty of $\pm 8\%$ was cited for the coaxial gauge measurements but an overall experimental uncertainty was not given.

B.   Other Relevant Sources of High-Enthalpy Convective Aeroheating Data

Other sources for high-enthalpy aeroheating data sets exist that may be of use in defining uncertainties in nonequilibrium kinetic models even though these data were not obtained in pure CO_2 flows. These include, as previously noted, CO_2-Ar and air data from the ARC 42-Inch Shock Tunnel [5], air data from GASL-HYPULSE [6–8], and N_2 data from Caltech T5 [10].

Other blunt-cone aeroheating data were obtained in several facilities as part of the NATO AGARD Working Group 18 activity [15]. Although the primary purpose of this program was to obtain rarefied wake flow data [16], high-enthalpy forebody aeroheating data were also generated in two of the tests [17]: those conducted at DLR-high enthalpy shock-tunnel Göttingen (DLR-HEG) and CUBRC LENS.

The DLR-HEG tests was conducted on a 70 deg sphere-cone model with high-enthalpy runs in air, CO_2, and CO_2-N_2 mixtures. Unfortunately, explicit information regarding freestream specie mass
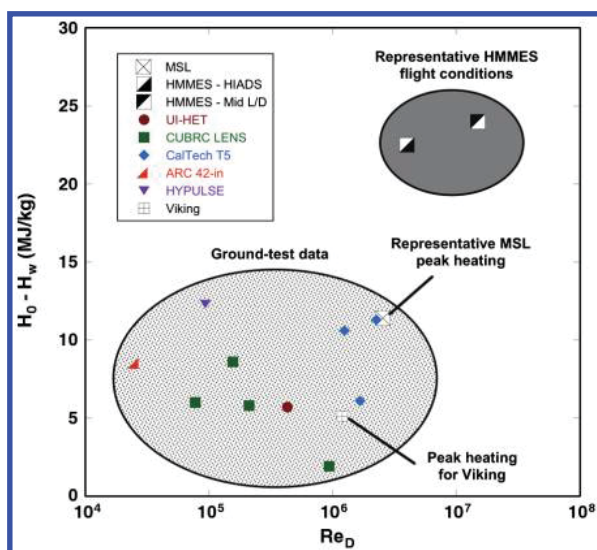

Fig. 6   Comparison of ground test and flight conditions.

Table 3 Forward reaction rate coefficients

No.	Reaction	A	B	C	Type	Third-party multiplier	Refs.
1	$CO + M \rightarrow C + O + M$	2.3×10^{20}	-1.00	1.29×10^5	Dissociation		[28]
2	$CO + O \rightarrow O_2 + C$	3.9×10^{13}	-0.18	6.92×10^4	Exchange		[29]
3	$CO_2 + M \rightarrow CO + O + M$	1.5×10^{25}	-2.50	6.60×10^4	Exchange	$\times 2$ for M = atoms	[30]
4	$CO_2 + O \rightarrow O_2 + CO$	2.1×10^{13}	0.00	2.78×10^4	Dissociation		[28]
5	$O_2 + M \rightarrow 2O + M$	2.0×10^{21}	-1.50	5.94×10^4	Dissociation	$\times 5$ for M = atoms	[29]

concentrations is incomplete in the documentation available [18–20]. Because it was not within the scope of this study to perform computations to determine facility operating conditions, these data were not analyzed. If such information could be obtained, these data should be factored into future work.

The CUBRC LENS AGARD-18 test was conducted on a 70 deg sphere-cone model in air and N_2 at enthalpies between 5 and 10 MJ/kg. Data were obtained [21] on both the blunted-cone forebody and in the wake on an instrumented sting.

III. Computational Methods

Flowfield solutions were generated at each test condition using NASA's LAURA and DPLR codes. These codes are the two primary numerical simulation tools employed by NASA for continuum hypersonic aerothermodynamic computations and extensive documentation and background material are available (e.g., [22–25]) for each code. Although there are some algorithmic and physical modeling differences between them, both are structured-grid Navier–Stokes solvers for flows with vibrational and chemical nonequilibrium. Past code-to-code comparisons have demonstrated good agreement between them for entry vehicle aerothermodynamic simulations relevant to HMMES, such as for the Mars Science Laboratory [26] and Fire II [27] missions.

In this study, the physical model employed was that of laminar flow, with two-temperature (translational and vibrational/electronic) representation and nonequilibrium chemical kinetics. A five-reaction chemistry model for the CO_2-CO-O_2-O-C system was used, with forward reactions as defined by the modified Arrhenius form of Eq. (1) and backward rates determined from the equilibrium constant definition via Eq. (2). The forward reaction coefficients are listed in Table 3. The carbon atom producing reactions (nos. 1 and 2) were included in this set for completeness; however, these reactions were found to be negligible for the range of test conditions considered:

$$k_F = A \times T^B \times \exp(-C/T) \text{ units of } \left(\frac{cm^3}{gmol\text{-}s}\right) \qquad (1)$$

$$k_B = \frac{k_F}{K_C} \text{ units of } \left(\frac{cm^6}{gmol^2\text{-}s}\right) \quad \text{or} \quad \left(\frac{cm^3}{gmol\text{-}s}\right) \qquad (2)$$

For the comparisons with experimental data, the freestream boundary conditions were taken from the published facility test conditions. The wall temperature boundary condition was set to a constant 300 K value; although heat transfer rates for these cases can be very high, the facility run times were in the millisecond to microsecond ranges, over which time the increase in wall temperature was negligible with respect to the boundary-layer edge temperatures. A surface catalysis boundary condition was also required. Several surface catalysis model options were employed: a noncatalytic option, a fully catalytic option (forces atoms to recombine to homogenous diatomics) and a "supercatalytic" option, in which recombination to 100% CO_2 is enforced at the surface. The choice of wall catalysis model has been shown to have a large effect on sensitivity of aeroheating predictions [4] but, unfortunately, as discussed in [3], there are little data available at low temperatures (such as generated in these tests) on catalysis effects for CO_2 reactions to help justify the selection of a particular catalysis model.

IV. Assessment of Experimental–Computational Comparisons

A. Surface Heat Transfer Comparisons

Comparisons were made between the LAURA and DPLR predictions and the experimental heat transfer data for each test condition. These comparisons are shown in Figs. 7–17 and are ordered in terms of increasing total enthalpy over the whole set of data, not just on a facility-by-facility basis. In each figure, the experimental data are shown with error bars of $\pm 15\%$. This value is purely a nominal figure used as a consistent reference and is not derived from the published reports; the actual stated experimental uncertainties varied from approximately 5 to 15% as discussed previously. For the computational results, predictions are shown for the noncatalytic, fully catalytic, and supercatalytic wall boundary condition options. LAURA and DPLR results were generally
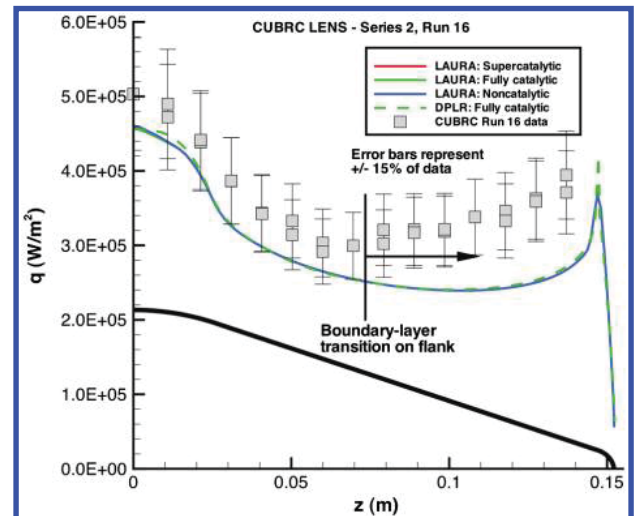

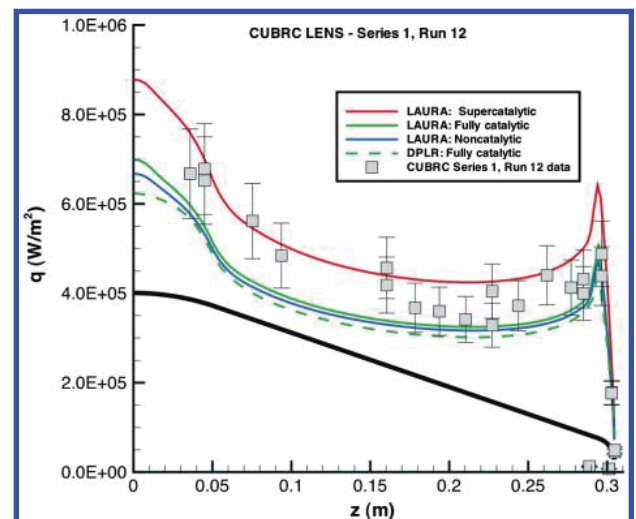**Fig. 7 CUBRC LENS I Reflected Shock Tunnel: Series 2, run 16, 1.9 MJ/kg case.**

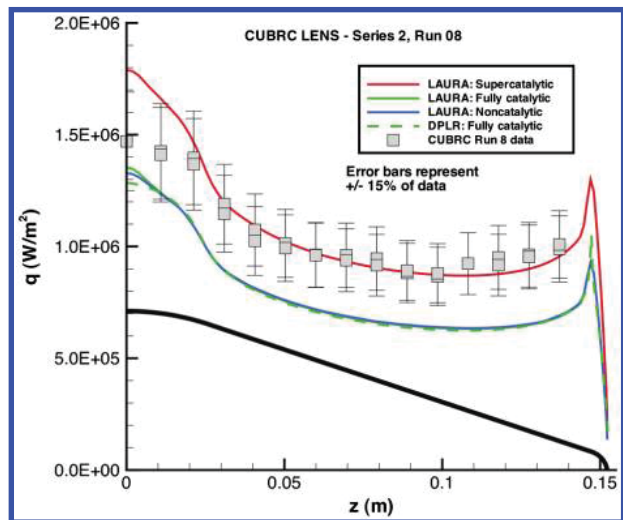**Fig. 8 CUBRC LENS I Reflected Shock Tunnel: Series 1, run 12, 5.1 MJ/kg case.**

Fig. 9 CUBRC LENS I Reflected Shock Tunnel: Series 2, run 8, 5.6 MJ/kg case.
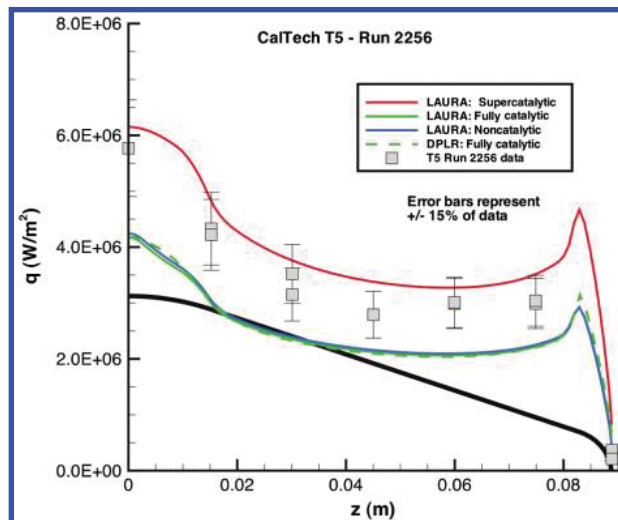

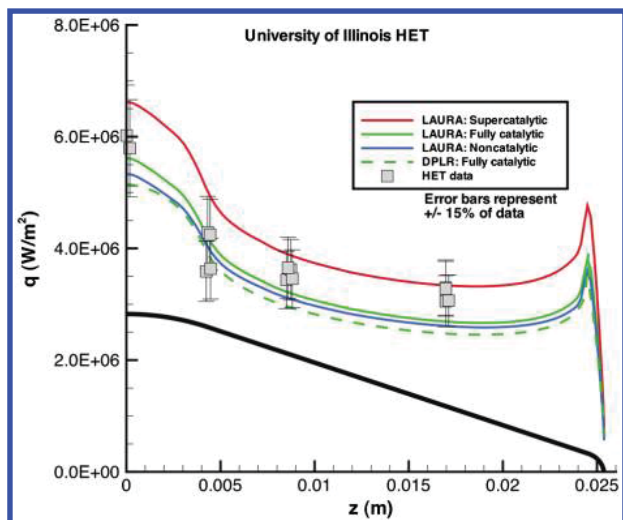**Fig. 12 Caltech T5 Reflected Shock Tunnel: Run 2256, 6.1 MJ/kg case.**

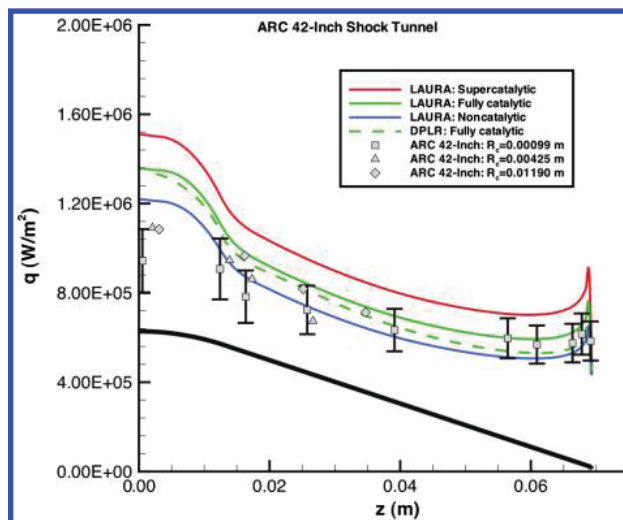**Fig. 10 University of Illinois HET Expansion Tube:5.7 MJ/kg case.**

Fig. 13 ARC 42-Inch Shock Tunnel: 8.5 MJ/kg case.

consistent with differences between them being much smaller than the differences produced by selection of the wall catalysis boundary condition. Thus, to maintain clarity on the plots, only the fully catalytic DPLR results will be shown along with the LAURA results for each boundary condition.

With the exception of the GASL HYPULSE case (which is the highest enthalpy condition), the current comparisons between predictions and measurements are similar to the comparisons previously published for each study. For the GASL HYPULSE case (Fig. 17), there is a large overprediction of the data in the current study
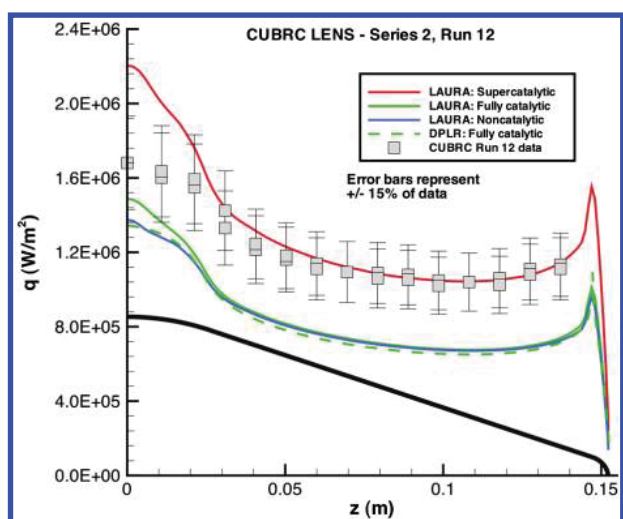
Fig. 11 CUBRC LENS I Reflected Shock Tunnel: Series 2, run 12, 6.0 MJ/kg case.
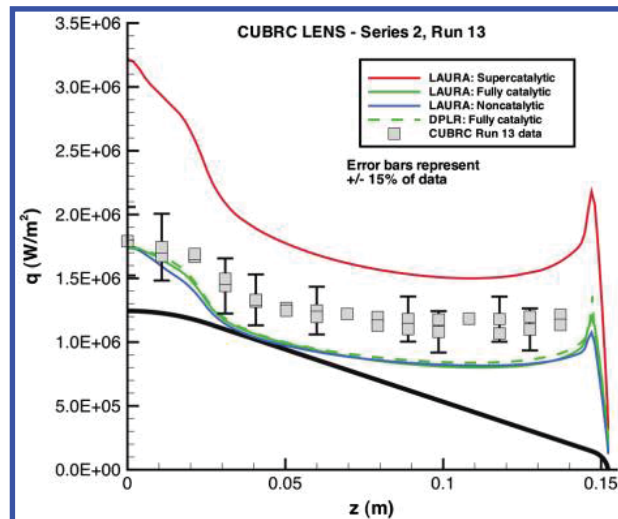
Fig. 14 CUBRC LENS I Reflected Shock Tunnel: Series 2, run 13, 8.6 MJ/kg case.
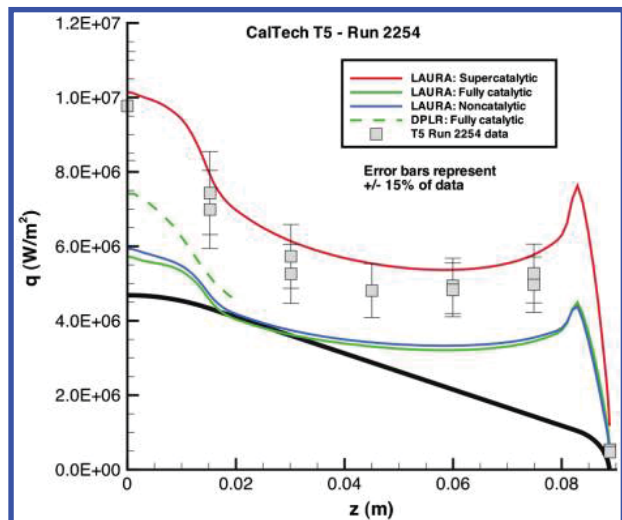
Fig. 15   Caltech T5 Reflected Shock Tunnel: Run 2254, 10.6 MJ/kg case.
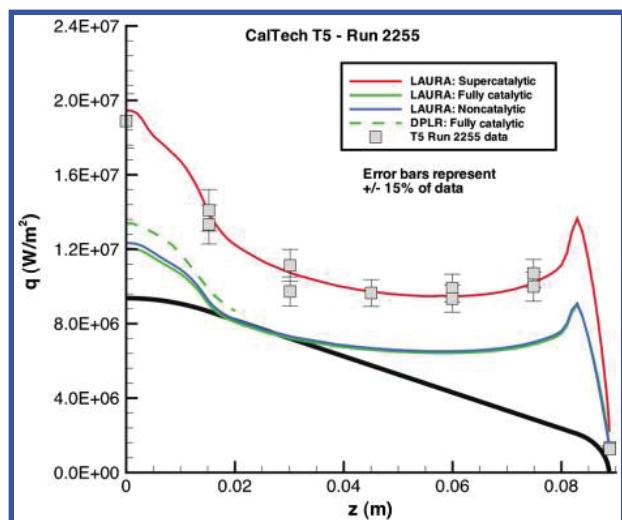

Fig. 16   Caltech T5 Reflected Shock Tunnel: Run 2255, 11.3 MJ/kg case.

that was not evident in the original comparisons. This difference was traced to the chemical–kinetic models employed. In the original study, explicit forward and backward reaction rates were specified as per Evans et al. [31], whereas in the current study, the backward rates
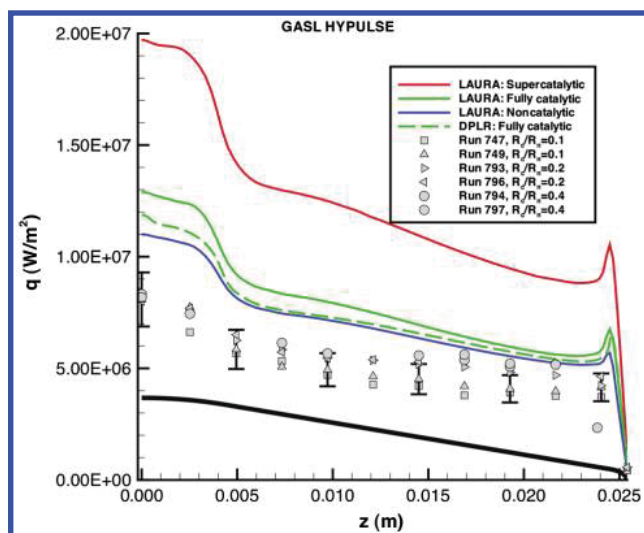

Fig. 17   GASL HYPULSE Expansion Tube: −12.3 MJ/kg case.
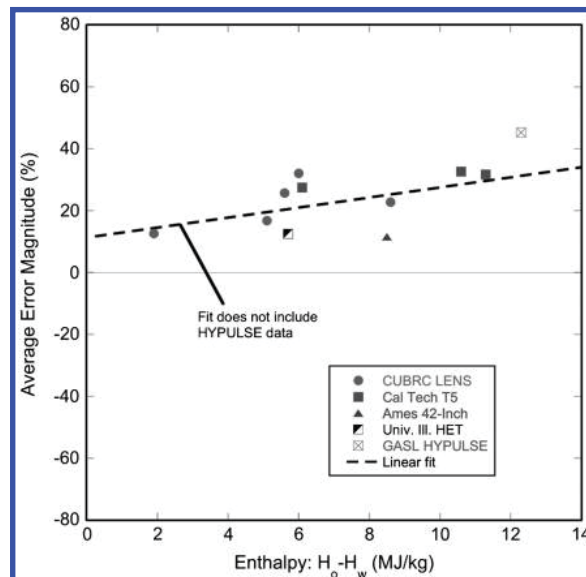

Fig. 18   Comparison of noncatalytic predictions with data (averaged error magnitude).

were determined from the definition of the equilibrium constant (e.g., [32]). When the chemistry models employed in [6–8] were substituted into LAURA, similar agreement with the experimental data was observed. This observation is not to intended to imply that one model or the other is "correct," but merely to identify the cause of a discrepancy between current and previous comparisons.

The differences between prediction and measurement shown for each of the gauges in Figs. 7–17 were averaged for each case to determine an overall uncertainty for that case. Averages were generated for supercatalytic and noncatalytic comparison in terms of both the average magnitude (absolute value) of the differences between prediction and measurement and the average of the signed (positive/negative) differences. These averages are plotted in Figs. 18–21 vs total enthalpy. From these figures, several general observations can be made:

1) The average magnitude per case of the differences between noncatalytic predictions and experimental data varied between 15 and 45%.

2) The average magnitude per case of the differences between supercatalytic predictions and experimental data varied between approximately 5 and 30%, with the exception of a 148% difference for the GASL HYPULSE case. Upon review of a draft of this paper by the operators of HYPULSE,[‡] it was indicated that the published results from this test may contain a data reduction error that produced erroneously high heating values. However, time limitations preclude reviewing and revising these data in the present publication.

3) The noncatalytic predictions averaged from approximately 1 to 35% *lower* than the data per case, expect for the GASL HYPULSE case where the predictions were 45% *higher* than the data.

4) The supercatalytic predictions averaged from 5 to 35% *higher* than the data per case, with the exception of a 148% overprediction for the GASL HYPULSE case and the underprediction for the low-enthalpy CUBRC LENS case.

5) A linear fit can be made for any of the average comparisons to show that the differences increase with total enthalpy. However, the quality of such fits is questionable given the small number of data points available and the skew resulting from the very large differences for the GASL HYPULSE case.

From these results, it is tempting to conclude that the supercatalytic boundary condition is appropriate because it provides the closest agreement with the data, with the exception of the GASL HYPULSE case, which could be eliminated as an outlier point (and is subject to possible revision due to data reduction error as noted previously). In fact, for NASA's MSL mission, this conclusion was

_____
‡From private communication with Ching-Yi Tsai, ATK (Aug. 2011).

Fig. 19   Comparison of noncatalytic predictions with data (averaged signed error).
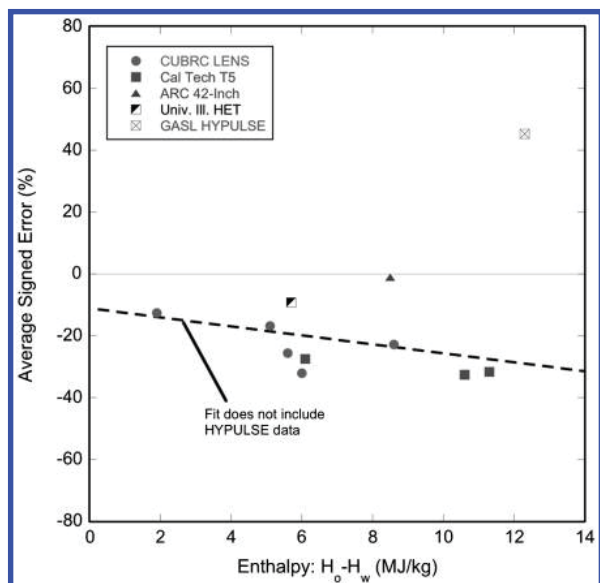

Fig. 21   Comparison of supercatalytic predictions with data (averaged signed error).

applied because the supercatalytic option provides the most design conservatism [33].

However, although possibly appropriate as a vehicle design paradigm, such a conclusion cannot be applied to a rigorous uncertainty analysis. Other evidence must also be considered. First, that the limited set of data on CO_2 surface catalysis do not support [3] the supercatalytic model for metallic surfaces at low temperatures. Second, that the HYPULSE data were obtained on models fabricated from Macor ceramic, which would be expected to show even less catalytic efficiency than a metallic model; thus, this test may provide a distinctly different physical environment than the others and cannot be immediately dismissed. Third, that the freestream environment of the GASL HYPULSE test (and also the University of Illinois HET test) was generated in a significantly different manner than the CUBRC LENS, Caltech T5, and Ames 42-Inch Shock Tunnel tests; the first two facilities operate as shock-expansion tunnels, whereas the other three operate as reflected shock tunnels. As discussed in [34], there is considerable uncertainty as to the vibrational nonequilibrium state of the freestream in reflected shock tunnels, which could produce significant uncertainties in the results surface heat transfer measurements. And finally, as will be shown in the next section, regardless of surface catalysis model selected, major
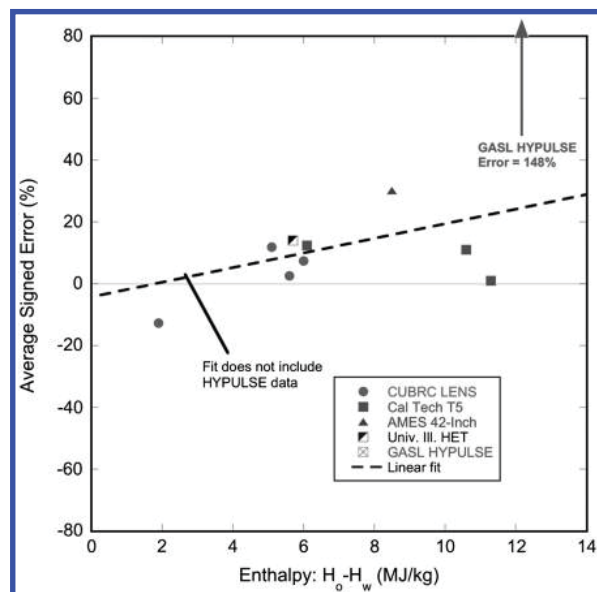
differences were also observed in the comparisons between predicted and measured shock shapes. Such flowfield differences cannot be a function of surface catalysis, thus there must be other uncertainty factors to consider.

B.   Shock-Shape Comparisons

Comparisons were made between the predicted and measured shock shapes (with the exception of Caltech run 2256 for which no image was available) as shown in Figs. 22–30. The differences between predicted and measured shock standoff distances at the nose are shown in Fig. 31 with respect to total enthalpy and in Fig. 32 with respect to freestream density. With the exception of the lowest enthalpy CUBRC LENS case (series 2, run 16) and perhaps the ARC 42-Inch case, there were large differences between the predicted and measured shock shapes for all cases. Shock standoff distances were underpredicted for the CUBRC LENS and GASL HYPULSE cases and overpredicted for the Caltech T5 and University of Illinois HET cases (the available image quality was too low for assessment of the ARC 42-Inch Shock Tunnel case). These comparisons suggest fundamental differences between actual and computed chemical and
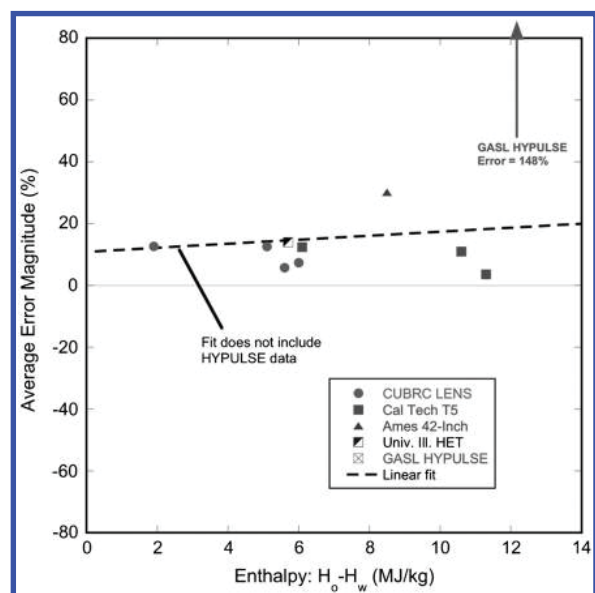

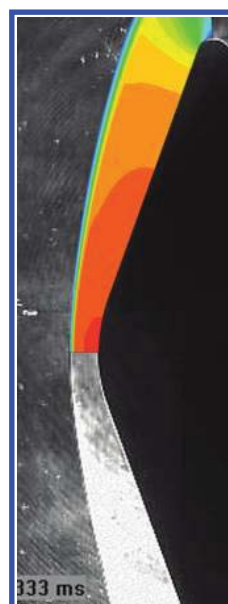Fig. 20   Comparison of supercatalytic predictions with data (averaged error magnitude).

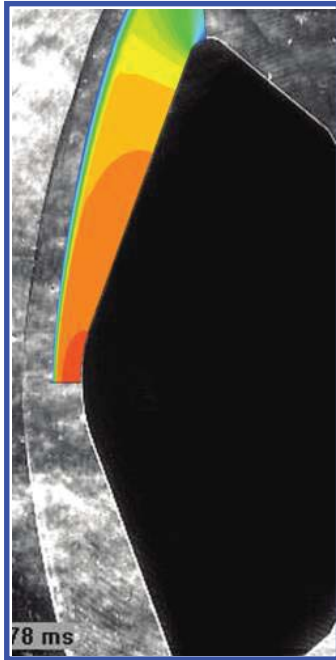Fig. 22   CUBRC LENS I Reflected Shock Tunnel: Series 2, run 16, 1.9 MJ/kg case.

Fig. 23 CUBRC LENS I Reflected Shock Tunnel: Series 2, run 8, 5.6 MJ/kg case.

Fig. 25 CUBRC LENS I Reflected Shock Tunnel: Series 2, run 12, 6.0 MJ/kg case.

vibrational relaxation rates, which would strongly influence the predicted surface heating rates. Thus, it cannot be said for certain whether the differences in measured and predicted heating rates were due to the surface catalysis, chemical and vibrational rates (or both), or other factors. And, because high-enthalpy facilities' freestream conditions are typically determined through a combination of diagnostic measurements and numerical methods, it is also possible that the freestream conditions were not accurately characterized. This possibility is more likely for the reflected shock tunnels, as discussed in [14,34].

Although the focus of this study is primarily on heat transfer uncertainties, the prediction of shock shapes also affects aerodynamic uncertainties. The shock shape is an indictor of the surface pressure distribution and thus of the forces and moments resulting from the integration of that pressure distribution. It has been shown [35] that the use of different models (Camac [36] and Millikan–White [37]) for vibrational relaxation rates of the polyatomic CO_2 molecule produces an uncertainty in the trim angle of a degree or more for the MSL-entry
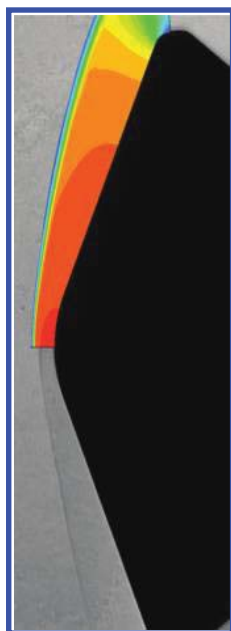
vehicle, which is a significant level for a mission that requires precision entry. The differences in predicted and measured shock shapes for the cases in this study were much larger than those generated for the MSL case in [34], and so the aerodynamic uncertainties can be expected to be large; however, there are no data available for comparisons.

C. Overall Assessment of Comparisons

Without attempting to assign the cause to either experimental or computational methods, this survey reveals that very large differences exist between the two with respect to convective aeroheating rates and flowfield shock shapes for high-enthalpy CO_2 flows. Differences in heat transfer rates varied between 15 and 148% and were strongly influenced by the selection of surface catalysis models for the computations. Shock standoff distance comparisons revealed differences ranging from 50% underprediction to 50% overprediction.
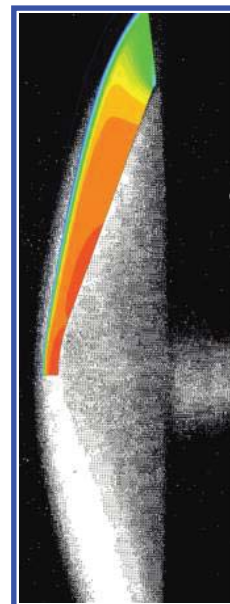

Fig. 24 University of Illinois HET Expansion Tube: 5.7 MJ/kg case.

Fig. 26 ARC 42-Inch Shock Tunnel: 8.5 MJ/kg case.

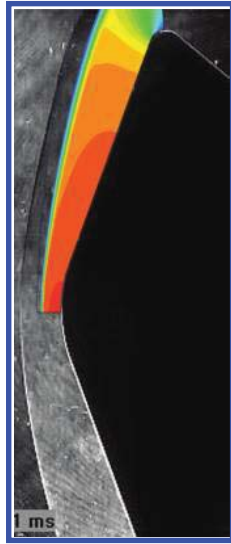**Fig. 27   CUBRC LENS I Reflected Shock Tunnel: Series 2, run 13, 8.6 MJ/kg case.**

Fig. 29   Caltech T5 Reflected Shock Tunnel: Run 2255, 11.3 MJ/kg case

These comparisons are startlingly poor and their implications for Mars exploration missions must be considered. First, in historical context, is the successful Viking mission. Viking peak heating conditions were on the low range of these data, where the uncertainty in heating might be assigned a "reasonable" value in the range of ±20% based on these comparisons. Off course, neither the data sets reviewed herein nor the computational techniques employed existed when that mission was developed. Instead, analytical methods were applied with high levels of conservatism.

In contrast, the MSL mission, for which most of these data sets were developed, is at the high end of the test range. Noncatalytic predictions were up to ∼35% lower than the experimental data, whereas supercatalytic predictions were up to ∼35% higher (excepting the GASL HYPULSE case). It is fortunate that, in fact, the supercatalytic model was employed in the design process because it overpredicts all experimental data except a single low-enthalpy condition.

Looking to the future, HMMES-class missions will experience enthalpies well beyond any existing test data. Because HMMES missions are outside the range of the test data, it cannot safely be assumed that the supercatalytic assumption will provide sufficient conservatism for aeroheating predictions. Additionally, the fact that

the predicted and measured shock shapes differ indicates that other phenomena beside wall catalysis are not being modeled properly and may also contribute to aeroheating uncertainties. And, of course, these differences in shock shapes produce an aerodynamic uncertainty that cannot be assessed because there are no relevant force-and-moment data against which to compare predictions.

It is a requirement of this study that some numerical values be assigned to the computational aeroheating uncertainty of the state-of-the-art tools used by NASA for Mars-entry problems. Although such an assessment is recognized as being overly simplistic, it at least provides a starting point for consideration of the issue. Thus, based on the comparisons presented in Figs. 7–17, approximate uncertainty estimates for laminar, convective aeroheating have been made in terms of total enthalpy. Because of the previously noted doubts as to the appropriateness of the supercatalytic boundary conditions, these estimates are based on the averaged error magnitude resulting from the noncatalytic boundary condition: 1) for low enthalpy (<5 MJ/kg), ±15% uncertainty; 2) for moderate enthalpy (5–10 MJ/kg), ±30% uncertainty; and 3) for high enthalpy (10–20 MJ/kg), ±60% uncertainty.

Fig. 28   Caltech T5 Reflected Shock Tunnel: Run 2254, 10.6 MJ/kg case.

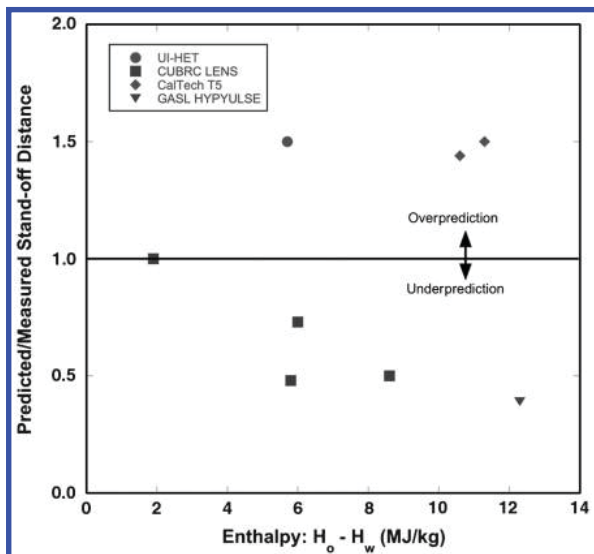**Fig. 30   GASL HYPULSE Expansion Tube: Run 749, 12.3 MJ/kg case.**

Fig. 31 Comparison of predicted and measured shock standoff distances vs enthalpy.

Of course, the overall aeroheating uncertainty must be considerably higher than these values for the laminar, convective uncertainty. Turbulent aeroheating augmentation, shock-layer radiation, and TPS roughness and ablation will also contribute to the aeroheating environment. Although some relevant test data do exist on these phenomena, an assessment of their effects cannot be performed until the cause or causes of the existing discrepancies between predictions and measurements illustrated herein have been resolved. Furthermore, these estimates reflect only the macroscopic comparisons between predictions and data and do not in any way address the underlying uncertainties in the physical models employed in the predictions.

D. Deficiencies in Current Experimental and Computational Methodologies

Despite more than 30 years of Mars exploration missions, there has been no comprehensive program to obtain benchmark-quality experimental data on aeroheating in CO_2-dominated flows, nor has there been a parallel effort to develop and validate computational methods for Martian entry conditions. Although it is true that some testing has been performed in the last decade to support the MSL program, these tests have produced more questions than answers. On the computational side, NASA's two state-of-the-art computational

fluid dynamics (CFD) tools, DPLR and LAURA, are based on the same 1980s–1990s-era physical models and differ mainly in algorithmic applications. For a HMMES-class mission to be possible, the current computational uncertainties levels must be better defined and must be greatly reduced. Several avenues of research must be followed to accomplish this task.

First is the acquisition of flight data. Aerothermodynamic instrumentation must be a requirement for any and all future Mars missions. Both Mars Viking [38,39] and Mars Pathfinder [40] carried some instrumentation, however, the data obtained were of limited utility. On a more positive note, the MSL mission will carry a comprehensive flight instrumentation package [41,42].

Second is the development and validation of higher-fidelity computational models for physical phenomena, especially for nonequilibrium chemical and vibrational processes and chemical catalysis. Current models are based on the two-temperature approach [43] for translational and vibrational modes and have Arrhenius-form chemical rate expressions fitted to these temperatures (e.g., [29]). However, the validity of the two-temperature approach has been called into question [44] and investigations of new thermophysical models have begun (e.g., [45,46]). It is important that development of such models take into account not only flight-relevant conditions, but also ground-test conditions to provide some anchor point for model validation.

Finally, more ground-test data are required and the requirements for future testing will be dealt with in greater depth. With respect to the existing data sets, several deficiencies can be identified that must be addressed in future testing:

1) As detailed in Table 1, data were obtained across a fairly wide range of conditions in the five different facilities, but there was no overlap of test conditions between the facilities. It is most notable that densities in the Caltech T5 test, in which shock standoff distances were overpredicted, were an order of magnitude higher than those of the CUBRC LENS test, in which shock standoff distances were underpredicted. This observation suggests a possible connection because chemical and vibrational processes will be influenced by density, however, other factors must also be considered. An overlap in test conditions in multiple facilities should be a requirement for future testing.

2) Testing was not conducted in any of the individual facilities across a wide enough range of test conditions to generate significant differences in the flowfield environments in any one facility. Future tests should span an enthalpy range in each facility sufficient to encompass both perfect (or near-perfect) gas and chemically reacting gas conditions in order produce a wide range of chemical reaction rates, as well as densities sufficient to encompass both equilibrium and nonequilibrium conditions. This requirement will help identify trends in the physical processes (such as catalysis, vibrational relaxation, and chemical reaction rates) and to validate the operational characteristics of the facilities.

3) The heat transfer instrumentation types were not consistent from facility to facility. Thin-film gauges, coaxial thermocouples, surface thermocouples, and calorimeters were all employed. Although some variation in instrumentation is desirable to provide independent quality checks, at least one common type of instrumentation should be employed in all tests.

4) Although the evidence is not conclusive, it has been hypothesized (e.g., [34]) that the operating conditions of the reflected-shock tunnels (Ames 42-Inch, CUBRC LENS, Caltech T5) may have been influenced by nonequilibrium vibrational and/or chemical excitation that was not properly characterized. Theoretically, shock-expansion tunnels will be less prone to such difficulties and testing should be concentrated on such facilities, although the use of reflected-shock tunnels should be not completely rejected. However, the process of characterizing the flowfield in any high-enthalpy facility is complicated by the fact that the CFD tools for which validation data are sought are also being used to determine the freestream conditions of the tests being performed to generate validation data. Thus, an iterative process will be required to develop and validate models for both the facility operational processes and the resulting flow around the test article.
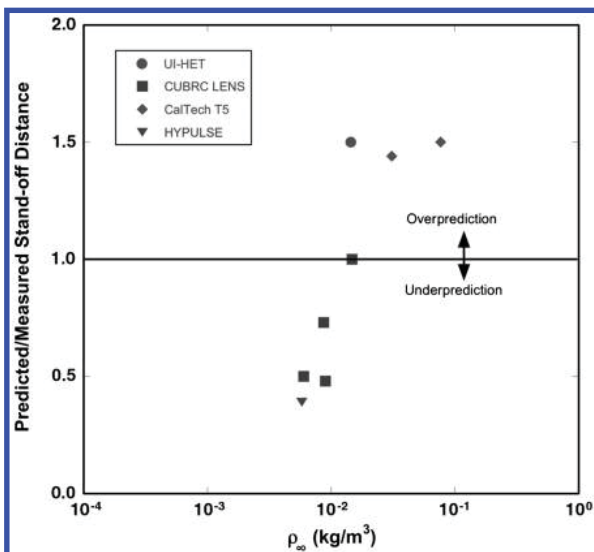

Fig. 32 Comparison of predicted and measured shock-standoff distances vs density.

5) The catalytic properties of the wind-tunnel models were not conclusively established. The tentative assumption is that the metallic models used in all tests except GASL HYPULSE were noncatalytic. For the HYPULSE test, this assumption is even more credible because the models were fabricated from Macor ceramic. It should be a requirement for future testing that independent analyses are conducted to determine the catalytic properties of both the wind-tunnel model materials and of the instrumentation (i.e., thin-film or thermocouple surfaces).

6) The thermophysical properties of the wind-tunnel model materials (i.e., thermal diffusivity and thermal conductivity) must be better characterized. Uncertainties in these properties have a direct linear effect on the conduction analyses performed to determine heat transfer rates from the measured temperature-time histories. Unfortunately, this information is rarely documented in test reports, even though some studies have identified significant uncertainties in the available literature (e.g., [8,47]).

7) All testing to date has been performed at "cold-wall" conditions where wall temperatures remain relatively unchanged (with respect to flowfield total temperature) due to the brief duration of high-enthalpy facility runs. If possible, some testing should be performed with models preheated to an elevated temperature; this requirement may provide some insight into chemical and catalytic behavior at the wall.

V. Conclusions

Future Mars exploration missions under consideration by NASA will require the development of high-mass mars-entry Systems. These systems will have masses an order of magnitude greater than those of previous missions and will experience much more severe aerothermodynamic entry environments. To support the future development of these systems, a survey was conducted to identify sources of high-enthalpy, CO_2 aerothermodynamic data that could be used to help define computational uncertainties in state-of-the-art flowfield prediction tools employed by NASA.

Comparisons were performed between these experimental data and computational predictions generated for this study. Large differences were found to exist for both surface heat transfer rates and flowfield shock shapes. Estimates for the uncertainty in computational aeroheating predictions ranged from $\pm15\%$ at low enthalpy (<5 MJ/kg) to $\pm60\%$ at high-enthalpy (>10 MJ/kg). However, the scope of the data sets was not sufficient to perform rigorous uncertainty analyses. Several factors were found to influence these results, including the correct modeling of surface catalysis, the proper definition of freestream test conditions, and numerical modeling of vibrational relaxation rates for CO_2. Large discrepancies in predicted and measured shock shapes were also identified. Although experimental aerodynamic data were not available to evaluate the integrated effects of these shock-shape differences, they are large enough to be of concern when accurate guidance for precision landing is required.

The results of this study are intended to aid in the development of guidelines for future NASA investments in experimental and computational research toward decreasing entry-vehicle design uncertainties and margins for future Mars missions. Specific requirements for future experimental aerothermodynamic testing have been provided. Additional research will be required to better define, and ultimately reduce, these uncertainties.

References

[1] Cianciolo, A. M., Davis, J. L., Komar, D. R. et al., "Entry, Descent and Landing Systems Analysis Study: Phase 1 Report," NASA TM-2010-216720, July 2010.

[2] Bose, D., Brown, J., Prabhu, D. K., Gnoffo, P., Johnston, C. J., and Hollis, B., "Uncertainty Assessment of Hypersonic Aerothermodynamics Prediction Capability," *AIAA Thermophysics Conference*, AIAA Paper 2011-3141, June 2011.

[3] Wright, M. J., Tang, C. Y., Edquist, K. T., Hollis, B. R., Krasa, P., and Campbell, C. A., "A Review of Aerothermal Modeling for Mars Entry Missions," *48th AIAA Aerospace Sciences Meeting*, AIAA Paper 2010-0443, Jan. 2010.

[4] Bose, D., Wright, M. J., and Palmer, G. E., "Uncertainty Analysis of Laminar Aeroheating Predictions for Mars Entries," *Journal of Thermophysics and Heat Transfer*, Vol. 20, No. 4, Oct.–Dec. 2006, pp. 652–662.
doi:10.2514/1.20993

[5] Stewart, D. A., and Chen, Y. K., "Hypersonic Convective Heat Transfer over 140-Deg Blunt Cones in Different Gases," *Journal of Spacecraft and Rockets*, Vol. 31, No. 5, Sept.–Oct. 1994, pp. 735–743.
doi:10.2514/3.26506

[6] Hollis, B. R., and Perkins, J. N., "High-Enthalpy Aerothermodynamics of a Mars Entry Vehicle, Part 1: Experimental Results," *Journal of Spacecraft and Rockets*, Vol. 34, No. 4, July–Aug. 1997, pp. 449–456.
doi:10.2514/2.3257

[7] Hollis, B. R., and Perkins, J. N., "High-Enthalpy Aerothermodynamics of a Mars Entry Vehicle, Part 2: Computational Results," *Journal of Spacecraft and Rockets*, Vol. 34, No. 4, July–Aug. 1997, pp. 457–463.
doi:10.2514/2.3258

[8] Hollis, B. R., "Experimental and Computational Aerothermodynamics of a Mars Entry Vehicle," NASA CR-201633, Dec. 1996.

[9] Wright, M. J., Olejniczak, J., Brown, J. L., Hornung, H. G., and Edquist, K. T.," Modeling of Shock Tunnel Aeroheating Data on the Mars Science Laboratory Aeroshell," *Journal of Thermophysics and Heat Transfer*, Vol. 20, No. 4, Oct.–Dec. 2006, pp. 641–651.
doi:10.2514/1.19896

[10] Olejniczak, J., Wright, M. J., Laurence, S., and Hornung, H. G., "Computational Modeling of T5 Laminar and Turbulent Heating Data on Blunt Cones, Part 1: Titan Applications," *43rd AIAA Aerospace Sciences Meeting and Exhibit*, AIAA Paper 2005-0176, Reno, NV, Jan. 2005.

[11] Hollis, B. R., Liechty, D. S., Wright, M. J., Holden, M. S., Wadhams, T. P., MacLean, M., and Dyakonov, A., "Transition Onset and Turbulent Heating Measurements for the Mars Science Laboratory Entry Vehicle," *43rd AIAA Aerospace Sciences Meeting and Exhibit*, AIAA Paper 2005-1437, Reno, NV, Jan. 2005.

[12] MacLean, M., Wadhams, T., Holden, M., and Hollis, B. R., "Investigation of Blunt Bodies with CO_2 Test Gas Including Catalytic Effects," *38th AIAA Thermophysics Conference*, AIAA Paper 2005-4693, Toronto, June 2005.

[13] MacLean, M., and Holden, M., "Catalytic Effects on Heat Transfer Measurements for Aerothermal Studies with CO_2," *44th AIAA Aerospace Sciences Meeting and Exhibit*, Reno, NV, AIAA Paper 2011-3141, Jan. 2006.

[14] Sharma, M., Swantek, A. B., Flaherty, W., Austin, J. M., Doraiswamy, S., and Candler, G. V., "Experimental and Numerical Investigation of Hypervelocity Carbon Dioxide Flow over Blunt Bodies," *Journal of Thermophysics and Heat Transfer*, Vol. 24, No. 4, Oct.–Nov. 2010, pp. 673–683.
doi:10.2514/1.49386

[15] Muylaert, J., Kumar, A., and Dujarric, C. (eds.), "Hypersonic Experimental and Computational Capability, Improvement and Validation," AGARD Advisory Rept. 319, Vol. 2, Dec. 1998.

[16] Moss, J. N., and Lengrand, J. C., "Rarefied Flow," *Hypersonic Experimental and Computational Capability, Improvement and Validation*, edited by Muylaert, J., Kumar, A., and Dujarric, C., AGARD Advisory Rept. 319, Vol. 2, Dec. 1998, Chap. 3.

[17] Deiwert, G. S., and Eitelberg, G. "Real Gas/Blunt Cone Phase II Report," *Hypersonic Experimental and Computational Capability, Improvement and Validation*, edited by J. Muylaert, A. Kumar, and C. Dujarric, AGARD Advisory Rept. 319 Vol. 2, Dec. 1998, Chap. 4.

[18] Kastell, D., Rosenhauer, M., Wollenhaupt, M., Müller T., Krek, R., Beck, W., and Eitelberg, G., "Study of Aerochemistry Around a 70-Deg Half Angle Blunted Cone in the High Enthalpy Shock Tunnel, Part 1:

Preparation of the Tests," DLR Rept. DLR-IB 223-95 C17, 1995.

[19] Kastell, D., Krek, R., Rosenhauer, M., Wollenhaupt, M., Müller, T., Beck, W., and Eitelberg, G., "Study of Aerochemistry Around a 70-Deg Half Angle Blunted Cone in the High Enthalpy Shock Tunnel, Part 2: Results," DLR Rept. DLR-IB 223-95 C41, 1995.

[20] Kastell, D., "Aerodynamik eines stumpfen Kegels in reagierender Überschallströmung," DLR Rept. 97-06, ISRN DLR-FB-97-06, 1997; "Aerodynamics of a Blunted Cone in Reacting Hypersonic Flows" (in English).

[21] Holden, M., Harvey. J., Body, I., George, J., and Horvath T., "Experimental and Computational Studies of the Flow over a Sting Mounted Planetary Probe Configuration," *35th Aerospace Sciences Meeting and Exhibit*, AIAA Paper 1997-0768, Reno, NV, Jan. 1997.

[22] Gnoffo, P. A., "An Upwind Biased, Point-Implicit Relaxation Algorithm for Viscous, Compressible Perfect-Gas Flows," NASA TP-2953, 1990.

[23] Mazaheri, Alireza, Gnoffo, P. A., Johnston, C. O., and Kleb, W., "LAURA Users Manual: 5.3-48528," NASA TM-2010-216386, Aug. 2010.

[24] Wright, M. J., Candler, G. V. and Bose, D., "Data-Parallel Line Relaxation Method for the Navier–Stokes Equations," *AIAA Journal*, Vol. 36, No. 9, Nov. 1998, pp. 1603–1609.
doi:10.2514/2.586

[25] Wright, M. J., White, T., and Mangini, N., "Data Parallel Line Relaxation (DPLR) Code User Manual Acadia-Version 4.01.1," NASA TM-2009-215388, Oct. 2009.

[26] Edquist, K. T., Dyakonov, A. A., Wright, M. J., and Tang, C. Y., "Aerothermodynamics Environments Definition for the Mars Science Laboratory Entry Capsule,"*45th AIAA Aerospace Sciences Meeting and Exhibit*, AIAA Paper 2007-1206, Reno, NV, Jan. 2007.

[27] Hash, D., Olejniczak, J., Wright, M. J., Prabhu, D., Pulsonetti, M., Hollis, B, Gnoffo, P., Barnhardt, M., Nompelis, I., and Candler, G., "FIRE II Calculations for Hypersonic Nonequilibrium Aerothermodynamics Code Verification: DPLR, LAURA and US3D," *45th AIAA Aerospace Sciences Meeting and Exhibit*, AIAA Paper 2007-0605, Reno, NV, Jan. 2007.

[28] Park, C., Howe, J. T., Jaffe, R. L., and Candler, G. V., "Review of Chemical-Kinetic Problems of Future NASA Missions, II: Mars Entries," *Journal of Thermophysics and Heat Transfer*, Vol. 8, No. 1, Jan.–March 1994, pp. 9–23.
doi:10.2514/3.496

[29] Park, C., Jaffe R. L., and Partridge, H., "Chemical-Kinetic Parameters of Hyperbolic Earth Entry," *Journal of Thermophysics and Heat Transfer*, Vol. 15, No. 1, Jan.–March 2001, pp. 76–90.
doi:10.2514/2.6582

[30] Fujita, K., Yamada, T., and Nobuyuki, I., "Impact of Ablation Gas Kinetics on Hyperbolic Entry Radiative Heating," *44th AIAA Aerospace Sciences Meeting and Exhibit*, AIAA Paper 2006-1185, Reno, NV, Jan. 2006.

[31] Evans, J. S., Schexnayder, C. J., and Grose, W. L., "Effects of Nonequilibrium Ablation Chemistry on Viking Radio Blackout," *Journal of Spacecraft and Rockets*, Vol. 11, No. 2, Feb. 1974, pp. 84–88.
doi:10.2514/3.62013

[32] Gnoffo, P. A., Gupta, R. N., and Shinn, J. L., "Conservation Equations and Physical Models for Hypersonic Air Flow in Thermal and Chemical Nonequilibrium," NASA TP-2867, Feb. 1989.

[33] Edquist, K. T., Dyakonov, A. A., Wright, M. J., and Tang, C. Y., "Aerothermodynamic Design of the Mars Science Laboratory Heatshield," *41st AIAA Thermophysics Conference*, AIAA Paper 2009-4075, San Antonio, TX, June 2009.

[34] MacLean, M., and Holden, M., "Numerical Assessment of Data in Catalytic and Transitional Flows for Martian Entry," *9th AIAA/ASME Joint Thermophysics and Heat Transfer Conference*, AIAA Paper 2006-2946, San Francisco, June 2006.

[35] Schoenenberger, M., Dyakonov, A., Buning, P., Scallion, W., and Van Norman, J., "Aerodynamic Challenges for the Mars Science Laboratory Entry, Descent and Landing," *41st AIAA Thermophysics Conference*, AIAA Paper 2009-3914, San Antonio, TX, June 2009.

[36] Camac, M., "CO2 Relaxation Process in Shock Waves," *Fundamental Phenomena in Hypersonic Flows*, edited by J. G. Hall, Cornell Univ. Press, Ithaca, NY, 1966, p. 195.

[37] Millikan, R. C., and White, D. R., "Systematics of Vibrational Relaxation," *Journal of Chemical Physics*, Vol. 39, No. 12, Dec. 1963, pp. 3209–3213.
doi:10.1063/1.1734182

[38] Edquist, K. T., Wright, M. J., and Allen, G. A., "Viking Afterbody Heating Computations and Comparisons to Flight Data," *44th AIAA Aerospace Sciences Meeting and Exhibit*, AIAA Paper 2006-0386, Reno, NV, Jan. 2006.

[39] Edquist, K. T., "Computations of Viking Lander Capsule Hypersonic Aerodynamics with Comparisons to Ground and Flight Data," *AIAA Atmospheric Flight Mechanics Conference and Exhibit*, AIAA Paper 2006-6137, Keystone, CO, Aug. 2006.

[40] Milos, F. S., Chen, Y. K., Congdon, W. M., and Thronton, J. M., "Mars Pathfinder Entry Temperature Data, Aerothermal Heating, and Heatshield Material Response," *Journal of Spacecraft and Rockets*, Vol. 36, No. 3, May–June 1999, pp. 380–391.
doi:10.2514/2.3457

[41] Gazarik, M. J., Wright, M. J., Little, A., Cheatwood, F. M., Herath, J. A., Munk, M. M., Novak, F. J., and Martinez, E. R., "Overview of the MEDLI Project," *IEEE 2008 Aerospace Conference*, IEEE, March 2008, pp. 1–12.

[42] Karlgaard, C. D., Beck, R. E., O'Keefe, S. A, Siemers, P. M., White, B. A., Engelund, W. C., and Munk, M. M., "Mars Entry Atmospheric Data System Modeling and Algorithm Development," *41st AIAA Thermophysics Conference*, AIAA Paper 2009-3916, San Antonio, TX, June 2009.

[43] Park, C., "Assessment of Two-Temperature Kinetic Model for Ionizing Air," *Journal of Thermophysics and Heat Transfer*, Vol. 3, No. 3, July 1989, pp. 233–244.
doi:10.2514/3.28771

[44] Park, C., "The Limits of Two-Temperature Model," *48th AIAA Aerospace Sciences Meeting*, AIAA Paper 2010-0911, Orlando, FL, Jan. 2010.

[45] Candler, G. V., Doraiswamy, S., and Kelley, J. D., "The Potential Role of Electronically-Excited States in Recombining Flows," *48th AIAA Aerospace Sciences Meeting*, AIAA Paper 2010-0912, Orlando, FL, Jan. 2010.

[46] Doraiswamy, S., Kelley, J. D., and Candler, G. V.," Analysis of Chemistry-Vibration Coupling in Diatomics for High-Enthalpy Nozzle Flows," *48th AIAA Aerospace Sciences Meeting*, AIAA Paper 2010-1570, Orlando, FL, Jan. 2010.

[47] Coblish, J. J., Coulter, S. M., and Norris, J. D., "Aerothermal Measurement Improvements using Coaxial Thermocouples at AEDC Hypervelocity Wind Tunnel No. 9," *45th AIAA Aerospace Sciences Meeting and Exhibit*, AIAA Paper 2007-1467, Reno, NV, Jan. 2007.

D. Bose
Guest Editor